

Novel Strontium Carbides Under Compression

Nikita Rybin,^{1,2} Evgeny Moerman,³ Pranab Gain,¹ Artem R. Oganov,¹ and Alexander Shepeev^{1,2}

¹*Skolkovo Institute of Science and Technology, Bolshoi bulvar 30, build.1, 121205, Moscow**

²*Digital Materials LLC, Medovaya 3, 143085, Moscow Region*

³*Molecular Simulations from First Principles e.V., D-14195 Berlin, Germany*

(Dated: March 13, 2025)

Exploring the chemistry of materials at high pressures has led to the discovery of previously unknown exotic compounds. Here, we systematically search for all thermodynamically stable Sr-C compounds under pressure (up to 100 GPa) using the *ab initio* evolutionary crystal structure prediction method. Our search led to the discovery of hitherto unknown phases of SrC₃, Sr₂C₅, Sr₂C₃, Sr₂C, Sr₃C₂, and SrC. The newly discovered crystal structures feature a variety of different carbon environments ranging from isolated C anions and C-dimers to exotic polyatomic carbon anions including chains, stripes, and infinite ribbons consisting of pentagonal C₅ and hexagonal C₆ rings. Dynamical stability of all predicted compounds is confirmed by phonons calculations. Bader analysis unravels very diverse chemistry in these compounds and bonding patterns in some of them can be described using Zintl-Klemm rule.

I. INTRODUCTION

Chemical reactions that defy conventional chemical intuition can happen under extreme conditions, resulting in the emergence of rich phase diagrams and materials possessing intriguing properties, since pressure is known to greatly affect the chemistry of elements and cause the formation of exotic compounds [1, 2]. Well-known examples of such reactions involve the formation of sodium chlorides [3], a stable compound of helium and sodium [4], platinum group metal nitrides [5], and superconducting metal hydrides [6]. Nowadays, experimental high-pressure techniques allow one to explore materials chemistry up to terapascal pressure [7] and hence, confirm or deny theoretical predictions of exotic (from the chemical perspective) compounds. State-of-the-art computational techniques are reliable for predicting which compounds might be formed under certain thermodynamic conditions [8, 9]. For example, evolutionary crystal structure prediction has led to the *in silico* discovery of transparent dense sodium, unexpected forms of sodium chloride, and various superconducting metal-hydrides, which were later confirmed experimentally. [3, 10, 11]

Among all compounds previously investigated at high pressure, a particular focus was given to carbon-containing materials. Carbon (C) itself has the ability to form sp, sp², and sp³-hybridized bonds and therefore exists in various allotropic forms, including known structures of graphite, diamond, graphene, fullerenes, nanotubes. [12–19] High pressure alters the bonding patterns of carbides and leads to the formation of compounds with unusual carbon environments. [20–22] There are a large number of metal carbides containing acetylide group (C₂ dimers) [23–28], less common is the allylenide group (C₃ unit). [29–32] For the binary systems Mg-C [33], Ca-C [34, 35], Y-C [36–38], and La-C [20], an *ab initio* struc-

ture searches predicted the formation of unusual metal carbides with exotic C₄, C₅ units, C₆ rings, and graphene carbon sheets.

Despite a thorough exploration of the chemical space of metal carbides in the past, recent experiments revealed several novel compounds in the Y-C and Ca-C systems [35, 37]. Motivated by these findings, we decided to construct a pressure-composition phase diagram of the Sr-C system. Compressed strontium shows unique structural and electronic properties [39, 40], but to the best of our knowledge, strontium carbides were not investigated under compression. Here, using a variable-composition structure prediction methodology the pressure-composition phase diagram of the Sr-C system was explored in order to fully understand the structural diversity and evolution of the C-C bonding types under high pressure in the Sr-C system. This resulted in several newly predicted stable stoichiometries (SrC₃, Sr₂C₅, Sr₂C₃, Sr₂C, Sr₃C₂, and SrC) with a diverse set of carbon anions: isolated C atoms in Sr₂C, dimers in Sr₃C₂ and SrC, linear trimers in Sr₂C₃, chains in SrC, stripes with five-membered (C-pentagons) rings in SrC₂. There are also infinite ribbons consisting of five-membered (C-pentagons) rings in SrC₃, ribbons consisting of C-pentagons in SrC₂, and ribbons made of C-pentagons and C-hexagons in Sr₂C₅. Here, we discuss structural and electronic properties of these compounds.

II. COMPUTATIONAL METHODOLOGY

Crystal structure prediction techniques allow one to determine pressure-dependent phase diagrams for a given chemical space and a set of thermodynamic conditions. Such methodology, called a variable-composition search, is not limited to the prediction of the ground state structure of a particular stoichiometry, but explores the whole chemical space of the system in a single calculation [41]. Recently, by exploring pressure-composition phase diagrams of Cu-F, Ag-F, and Nd-F, we have shown

* n.rybin@skoltech.ru

that a variable-composition evolutionary crystal structure search allows one to find new stable compounds even after fixed-composition searches were done [11, 42, 43].

Here, we used two crystal structure prediction codes, which both implement an idea of the evolutionary crystal structure prediction. One, is the field-leading crystal structure prediction package USPEX [44–46]. Another one, is our own python-based implementation of the *ab initio* evolutionary algorithm, which has a functionality to perform variable-composition search. We call this implementation Sputnik (Structure prediction using theoretical kristallography) and details of the implementation will be published elsewhere, but we have to mention that workflow management in Sputnik is done using the FireWorks functionality [47]. The theoretical basis under the Sputnik’s implementation is identical to the USPEX’s one and it is presented in [41, 45, 48].

The evolutionary searches were combined with structure relaxations and energy calculations using density-functional theory (DFT) within the Perdew–Burke–Ernzerhof (PBE) [49] exchange–correlation functional. In the case of Sputnik, DFT calculations were performed using the plane-waves QE (Quantum Espresso) package [50, 51], while in the case of USPEX, we used VASP (Vienna ab initio simulations) package [52], with the projector augmented plane wave method [53]. For the variable-composition structure search, the first generation of 160 structures was composed of randomly generated, symmetric unit cells containing up to 18 atoms [46, 54]. 70% of the next generation was obtained by applying variation operators (heredity, softmutation, lattice mutation) to the 70% of the lowest-energy structures of the previous generation, while the remaining 30% of the generation were generated randomly. The percentage of structures produced by each of the variation operators was dynamically adjusted on-the-fly, based on the performance of each operator [55]. During the structure search, each generation of structures was relaxed through a series of steps with increasing precision of calculation parameters (plane wave cutoff, k-points density, scf-cycle convergence threshold). In the last step, we did single-point calculations using a plane-wave energy cutoffs of 60 Ry (in the case of VASP the kinetic energy cutoff was set to 600 eV) and Γ -centered k -meshes with a reciprocal space resolution of $2\pi \times 0.05 \text{ \AA}^{-1}$ for the Brillouin zone sampling. In these calculations, no constraints on stoichiometries were imposed as long as the unit cell had no more than 18 atoms, and calculations were performed at 10, 25, 50, 75 and 100 GPa.

Once structure prediction with Sputnik and USPEX was done, we calculated the pressure-composition phase diagram with a resolution of 10 GPa, then we confirmed the dynamical stability of all novel structures with phonon calculations using the supercell approach and the finite displacement method [56], as implemented in the Phonopy package [57]. The electron localization function (ELF) was calculated for all the novel phases and

visualized using VESTA.[58] For aforementioned calculations we used VASP. Bader charge analyses was performed on total charge density obtained using VASP.[59–62] The structural information for all discovered compounds, band structures, and phonon dispersion curves are presented in the Supplementary Materials (SM).

III. RESULTS

To determine stable phases in a variable-composition system, it is convenient to use the convex hull construction. Phases located on the thermodynamic convex hull are stable with respect to decomposition into elemental Sr and C or other Sr-C compounds. All the values of the chemical potentials, delimiting the fields of stability of compounds, are derived directly from the convex hull. Consequently, the convex hull construction is the cornerstone of the variable-composition structure prediction, which determines the stability of compounds at particular thermodynamic conditions [41].

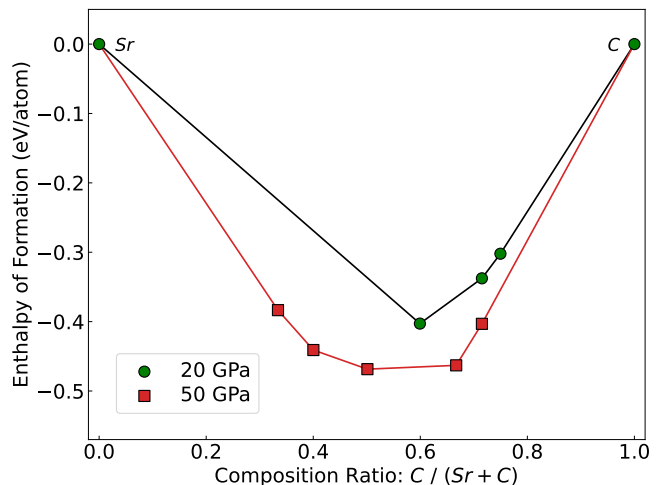


FIG. 1. Convex hull diagrams of the Sr-C system at 20 GPa (green disks) and 50 GPa (red squares). The enthalpy of formation H is defined as: $\Delta H(\text{Sr}_x\text{C}_y) = (H(\text{Sr}_x\text{C}_y) - xH(\text{Sr}) - yH(\text{C})) / (x + y)$.

Convex hulls of the Sr-C system at 20 GPa and 50 GPa are presented in Fig. 1. The pressure-composition phase diagram of the Sr-C system is shown in Fig 2, which was obtained by calculating enthalpies of the most stable structures for each composition at a given pressure (steps of 5 GPa were used). According to this diagram, we found eleven hitherto unknown phases in the Sr-C system. These compounds have the following stoichiometries: SrC_3 , Sr_2C_5 , SrC_2 , Sr_2C_3 , SrC , Sr_3C_2 , and Sr_2C (for some stoichiometries there are a couple of different structures). These structures are shown in Fig. 3. All crystallographic parameters are given in SM. For all the newly predicted structures, calculated phonon dispersion relations confirmed their dynamical stability (see SM Fig.S1.).

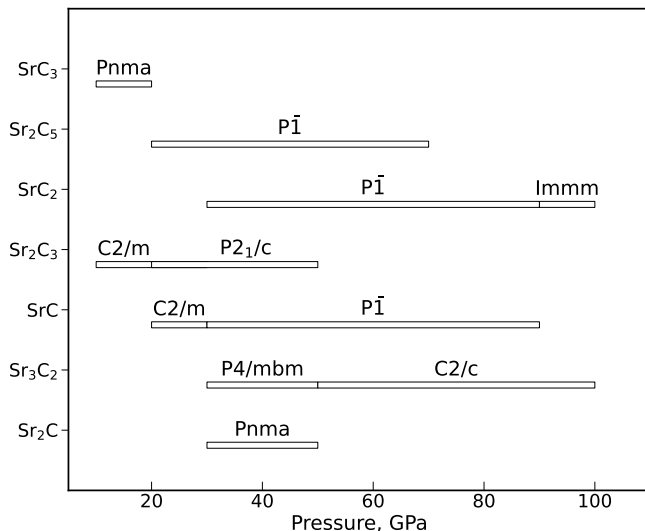


FIG. 2. Pressure-composition phase diagram for the Sr-C system.

The identified compounds have a variety of different carbon motifs, as demonstrated in Fig. 4. In the following, we consider the predicted phases in order of increasing carbon content. In order to analyze these structures, we recall that the length of the C - C bond depends on the bond order, and at 1 atm these lengths are 1.20 Å for the triple C-C bond, 1.33 Å for the double and 1.54 Å for the single C-C bond. Combining this knowledge with the results of Bader analysis, we unravel a very diverse chemistry.

According to our calculations Sr_2C crystallizes in the orthorhombic $Pnma$ space group. This structure is stable from 30 to 50 GPa, it is metallic, and contains isolated carbon atoms – the simplest carbon motif among all obtained compounds (see Fig. 3 (a)). Such stoichiometry was previously found in other metal-carbon compounds, for example, Ca_2C and Mg_2C . [34, 63] However, there is no reported theoretical or experimental data on Sr_2C . This metallic phase (see SM Fig. S2 (a)) can be represented as a methanide with an idealized charge distribution of $(\text{Sr}^{2+})_2\text{C}^{4-}$ and is in line with the Zintl concept.

Sr_3C_2 crystallizes in the tetragonal $P4/mbm$ space group at 30 GPa and transforms into a structure with a monoclinic $C2/c$ space group at 50 GPa. The structure of the newly identified Sr_3C_2 is of the U_3Si_2 type, a common arrangement found in silicides [64], borides [65], and intermetallic compounds [66]. Both structures are metallic and contain carbon dimers as presented in Figs. 3 (b, c). Carbides of calcium with this stoichiometry and space groups have been predicted previously [34]. In $P4/mbm$ - Sr_3C_2 phase, the structure contains doubly bonded C_2 groups (the C-C distance is 1.39 Å at 30 GPa) carrying an ideal charge of -4, receiving four electrons from Sr atoms. This leaves two electrons per C atom to establish C-C double bonds in the metallic framework. Hence, Sr_3C_2 (as well as Ca_3C_2) can be called an ethanide - at nor-

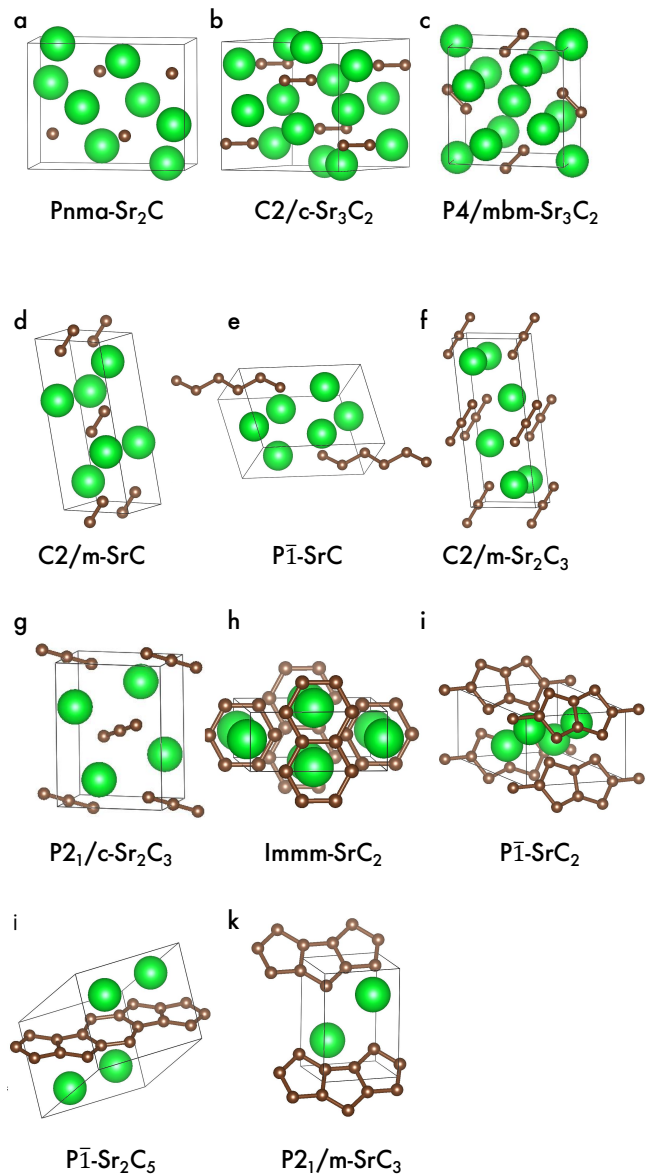


FIG. 3. Predicted crystal structures of stable Sr-C compounds. (a) $Pnma$ structure of Sr_2C . (b, c) $C2/c$ and $P4/mbm$ structures of Sr_3C_2 . (d, e) $C2/m$ and $P\bar{1}$ structures of SrC . (f, g) $C2/m$ and $P2_1/c$ structures of Sr_2C_3 . (h, i) $Immm$ and $P\bar{1}$ structures of SrC_2 . (j) $P\bar{1}$ structure of Sr_2C_5 . (k) $P2_1/m$ structures of SrC_3 . The green and brown spheres represent strontium and carbon atoms, respectively.

mal conditions ethanides are unknown unlike methanides and acetylides. A carbon atom with two additional electrons becomes isoelectronic with an oxygen atom, similar to the configuration found in the doubly bonded O_2 molecule. The Sr atoms are located in the same plane as the C_2 dumbbells, collectively forming the Cairo pentagonal tiling, which consists of $(\text{Sr})_2\text{C}_3$ pentagons (see Fig. 5 (a)). As shown in Fig. 5 (a), Sr atoms are four-fold coordinated by C atoms, with a Sr-C distance of 2.63 Å at 30 GPa. The electron localization function

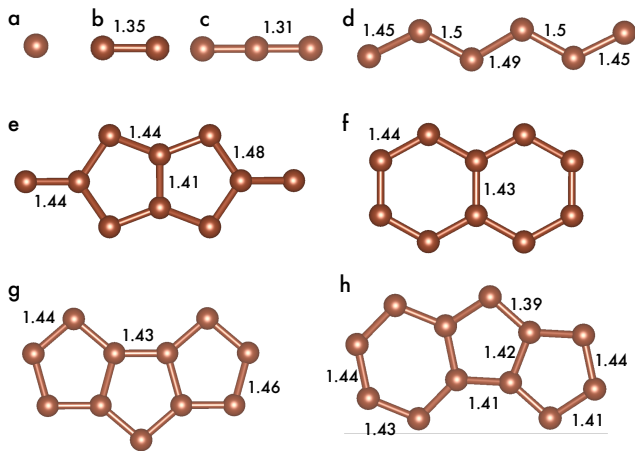


FIG. 4. Carbon patterns in the Sr-C system. (a) The isolated carbon anions in the $Pnma$ structure of Sr_2C . (b) Carbon dimers (dumbbells) observed in the $C2/c$ structure of Sr_3C_2 and $C2/m$ structure of SrC . (c) The carbon trimer occurs in the $C2/m$ structure of Sr_2C_3 . (d) Zigzag C_6 groups observed in $P\bar{1}$ structure of SrC at 50 GPa. (e) Carbon stripes in the $P-1$ structure of SrC_2 at 50 GPa. (f) Carbon ribbons with hexagonal C-rings in the $Immm$ structure of SrC_2 at 90 GPa. (g) Carbon ribbons with pentagonal C-environment in the $Pnma$ structure of SrC_3 at 20 GPa. (h) Carbon ribbons with pentagonal and hexagonal C-rings in the $P\bar{1}$ structure of Sr_2C_5 at 50 GPa.

indicates strong covalent bonding between the carbon atoms in the dimers and an ionic Sr-C interaction (see Fig. 5 (c)). Above 50 GPa the $P4/mbm$ - Sr_3C_2 transforms into $C2/c$ - Sr_3C_2 and the Cairo pentagonal tiling gets distorted. This distortion is accompanied by an increase in the C-C bond length of the C-dimers to 1.46 Å. Electron density maps in the plane containing the C_2 dimers reveal slightly higher ELF values between carbon atoms in the dimers of the $P4/mbm$ - Sr_2C_3 phase compared to the $C2/c$ - Sr_2C_3 phase (See SM Fig. S6). This suggests a higher bond order in the $P4/mbm$ - Sr_2C_3 dimer.

Metallic SrC exhibits two thermodynamically stable phases below 100 GPa. The low pressure monoclinic $C2/m$ phase on further compression transitions into a low-symmetry triclinic $P\bar{1}$ - SrC structure. At 30 GPa the structural formula of $C2/m$ is $Sr_2(C_2)$, featuring a doubly bonded C_2 group with a C-C bond length of 1.34 Å. This C_2 group carries an ideal charge of -4 (Bader charge -2.175), perfectly balancing the charge of two strontium atoms, and $C2/m$ - SrC is classified as an ethylenide. The $P\bar{1}$ - SrC structure is particularly intriguing due to its novel zigzag C-chain with C-C bond lengths ranging from 1.45 to 1.50 Å, implying bond orders between 1 and 2. The bond angles are 125.6° and 121.3°, which are remarkably close to 120° expected for sp^2 -hybridized carbon. The ELF maps clearly indicate strong covalent bonding between the carbon atoms and ionic bonding between Sr and C atoms (see SM Fig.S5).

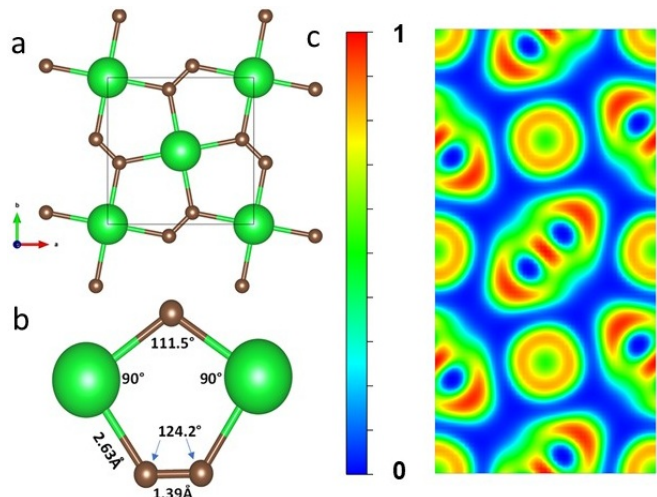


FIG. 5. Crystal structure of $P4/mbm$ - Sr_3C_2 at 30 GPa is depicted along with the computed electron localization function (ELF). Green and brown spheres represent strontium and carbon atoms, respectively. (a) Sr-C plane is a the Cairo pentagonal tiling formed by Sr and C atoms. (b) interatomic distances within the Sr-C plane. (c) 2D ELF of the $P4/mbm$ - Sr_3C_2 structure.

At lower pressures of about 10 GPa Sr_2C_3 becomes stable and crystallizes in the monoclinic $C2/m$ space group, and its structure contains allylenide-groups (C_3 units). Beyond 20 GPa, it transforms to the structure with $P2_1/c$ space groups, which is stable up to 50 GPa. These structures are the only semiconducting compounds found in this study (see SM Fig.S2). Usually, C_3 trimers are linear $[C=C=C]^{4-}$ groups with a C-C bond length of 1.34-1.35 Å (e.g., in Mg_2C_3), which is close to that in gaseous allene (1.335 Å) [67]. The structure of $C2/m$ - Sr_2C_3 at 20 GPa consists of Sr_2 layers connected by nearly linear, symmetric C_3 groups featuring double C-C bonds, with C-C distances measuring 1.31 Å. In this configuration, the ideal charge of the C_3 group is -4 (Bader charge -2.625), which precisely balances the total charge of the two Sr atoms in the formula, with one Sr atom having +1.314 Bader charge. The central carbon atom in the C_3 group should be neutral and the terminal carbons should have -2 charges as in gaseous allene. However, the central atom of the C_3 unit in Sr_2C_3 exhibits higher negative Bader charge of -1.225, while the terminal carbon atoms show lower Bader charges of -0.700 (see SM Tab. 1). This discrepancy is attributed to the significant ionic interactions between the Sr atom and the central carbon atom of the C_3 unit. This can be seen in the calculated 2D ELF of these structures (see SM Fig. S3).

SrC_2 becomes stable at 30 GPa and crystallizes in the low-symmetry $P\bar{1}$ space group. This structure contains exotic carbon stripes with fused five-membered C rings – the structural motif is presented in Fig. 4 (e). In this structure, two layers of Sr atoms are stacked between two layers of these stripes. The C - C distances within the C rings range from 1.41 to 1.48 Å at 30 GPa, indi-

ating the bonds intermediate between single and double. Upon compression, at 90 GPa there is a phase transition $P\bar{1}\text{-SrC}_2 \rightarrow Immm\text{-SrC}_2$. The $Immm\text{-SrC}_2$ structure contains extended carbon ribbons consisting of fused hexagonal C rings as presented in Fig. 4(f). These carbon ribbons are planar, with C-C distances of 1.43 Å and 1.44 Å at 90 GPa. The $Immm\text{-SrC}_2$ phase shares the same structure as the previously observed HP- CaC_2 ($Immm$) [34] and the predicted high-pressure YC_2 ($Immm$) [28]. In the low symmetry $P\bar{1}\text{-SrC}_2$ phase, the strontium atom is surrounded by 12 carbon atoms forming a heptagon and pentagon above and below the Sr atom (see Fig. 6 (a)). In the $Immm\text{-SrC}_2$ phase, the strontium atoms have 12 carbon neighbours arranged in a hexagonal prism with unequal bases (see Fig. 6 (c)). As was mentioned above, these C atoms are organized into poly-cyclic units of hexagonal rings, forming planar ribbons and as a result, the carbon atoms create exotic, one-dimensional extended poly-anions. The hexagon features two angles of 122.5° and four angles of 118.8° . These angles, being close to 120° , along with the similar C-C distances, suggest that the carbon atoms are sp^2 hybridized. The shared edges of hexagons in $Immm\text{-SrC}_2$ are slightly shorter (by approximately 0.01 Å) than the non-shared edges. This observation aligns with calculations in previously predicted isostructural high-pressure carbides (such as DyC_2 , CaC_2 , and YC_2), which show shorter shared edges by about 0.02–0.03 Å [68]. Bader charge analysis (See SM Tab. 1) suggests charge transfer from cationic Sr to C atoms. ELF maps of carbon ribbons in (see Fig. 6 (b, d)) suggest strong covalent bonds between carbon atoms and show localization of electrons on C-C bonds in pentagonal ribbons and hexagons.

Sr_2C_5 crystallizes in the low-symmetry space group $P\bar{1}$. C atoms in this structure feature extended ribbons consisting of C-pentagons and C-hexagons, as shown in Fig. 4(g, h). The C-C bond lengths range from 1.39 Å to 1.44 Å, indicating an intermediate bond order between single and double C-C bonds. In the Sr_2C_5 structure, one Sr atom has +1.248e Bader charge and is 13-fold coordinated, while another Sr atom has +1.202e Bader charge and is 12-fold coordinated (see Fig. 7(a)). In the fused C-hexagon and C-pentagon, carbon atoms are negatively charged. Therefore, it is evident that there is charge transfer from Sr to C atoms. Sr atom with 13-fold coordination is surrounded by the C-hexagon and a heptagon, while the Sr atom with 12-fold coordination is surrounded by the C-pentagon and a heptagon. In the C-hexagons, the four inner C atoms have three C-C covalent bonds each, while the two outer C atoms have two C-C covalent bonds and one lone pair of electrons each. The C-C bonds in the C-hexagon form two different angles α and β , where $\alpha=112^\circ$ and $\beta=124^\circ$. In C-pentagons, the inner four C atoms have three C-C covalent bonds, while the outer C atom has two C-C covalent bonds and a lone pair of electrons. The lone pairs of electrons can be seen in the 2-D electron localization function (see Fig. 7 (b)).

Finally, SrC_3 crystallizes in the $Pnma$ space group. In

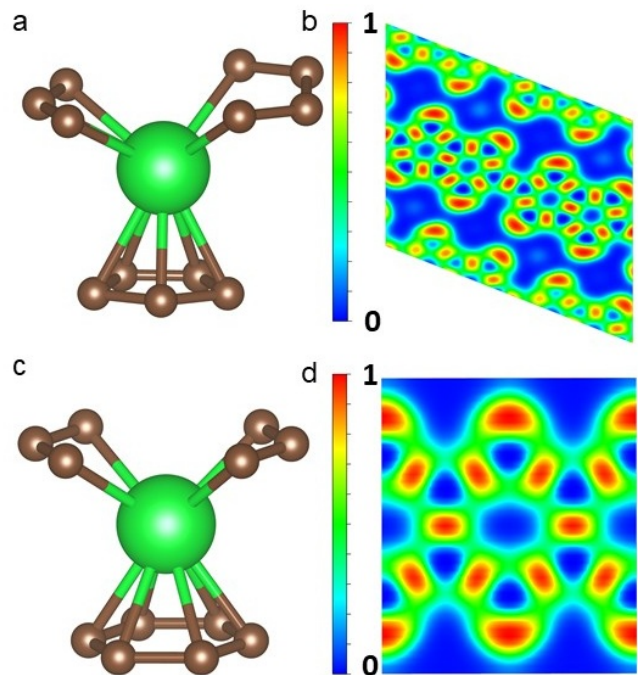


FIG. 6. The crystal structure of SrC_2 depicted along with the computed Electron Localization Function (ELF). Green and brown spheres represent strontium and carbon atoms, respectively. (a) Coordination of Sr atoms by C atoms, involving a pentagonal base, (b) 2D electron localization function (ELF) containing the pentagonal ribbons, (c) coordination environment of Sr atom in $Immm$ phase of SrC_2 (d) ELF containing the carbon ribbons in the $Immm\text{-SrC}_2$ phase.

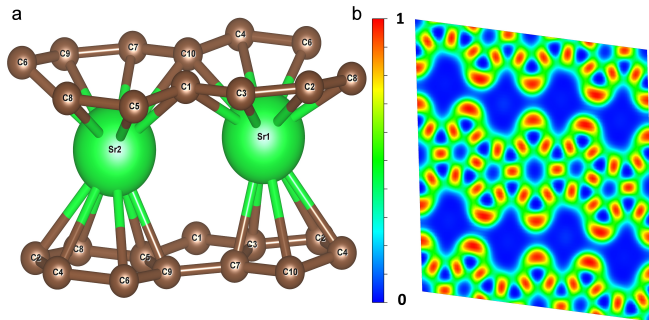


FIG. 7. (a) Coordination environment of the Sr atoms with the fused C-hexagons and C-pentagons in $P\bar{1}\text{-Sr}_2\text{C}_5$ (b) 2D ELF of the fused extended C-ribbons, consisting of C-hexagons and C-pentagons

this structure C atoms form infinite ribbons consisting of pentagonal carbon rings (see SM Fig. S4 (a)). Bader analysis indicates a charge transfer from strontium to carbon atoms, with strontium atoms acquiring a positive Bader charge of +1.343 (see SM Tab. 1). The carbon atoms, in contrast, have negative charges, with those not involved in ring fusion showing higher electron concentration. This is also evident in the 2D ELF plot (see SM Fig. S4 (b)).

In light of the appreciable diversity of the observed car-

bon motifs (see Figure 4), it is instructive to check if at least some of these configurations can be explained using conventional chemical wisdom. For that purpose, we investigated the applicability of the Zintl-Klemm (ZK) concept, originally conceived to rationalize bonding patterns of polyanions, to the newly identified strontium carbides. To assess the validity of the ZK rules, the average charge of a C-anion will be determined by assigning a formal +2 charge to the Sr atoms (Sr^{2+}) and imposing charge neutrality of the formal Sr_xC_y unit. For the example of Sr_2C this would lead to a formal charge of the carbon anion of -4 . By subsequently equating the structural motifs formed by that C-anion to the isoelectronic, neutral species, in the case of C^{4-} that would be a neon atom, the structure of the polyanion is inferred. Since neon is a noble gas, and Ne-Ne bonds cannot be formed, we expect no C-C bonds in Sr_2C , which we indeed observe. We performed this analysis for all herein discussed stoichiometries, which we have summarized in Table I. We find that for some of the strontium carbide compounds, namely Sr_2C , Sr_3C_2 and SrC , the C-anion structure is consistent with the motifs predicted from the ZK rule. This finding is also in agreement with a previous investigation of high-pressure Ca-C phases [34]. In the other cases, however, we find that the ZK concept cannot be directly applied, since for some stoichiometries including Sr_2C_3 , SrC_3 and Sr_2C_5 , the average formal charge on a C-atom would be fractional. Double and triple bonds also lead to exceptions from the ZK rule. A particularly noteworthy example is the case of SrC_2 , in which the carbon species would be isoelectronic to a nitrogen atom. As a consequence one would expect each carbon atom to form three covalent bonds. As illustrated in Figure 4, we find that the carbon polyanion in *Immm*- SrC_2 consists of planar, naphthalene-like arrangements. The planarity and the similarity of all C-C bond lengths in that polyanion suggests that that configuration is aromatic. This implies that most of the carbon atoms form one single and one double bond, so that the bonding of these atoms in *Immm*- SrC_2 is consistent with the ZK prediction. The two carbon atoms shared between the two rings, however, must then consequently have two single bonds and one double bond, which is not compatible with the isoelectronic N-atom. The same argument applies to the planar structure of the anion in the $P\bar{1}$ phase of SrC_2 , so that both SrC_2 phases are in contradiction with the ZK rule.

IV. CONCLUSION

In summary, we have produced the first complete pressure-composition phase diagram for Sr-C compounds at pressures up to 100 GPa. As a result we predicted eleven novel thermodynamically stable phases in the Sr-C system. Using electronic structure calculations and by performing Bader charge analysis we unraveled very diverse chemistry in these compounds. Carbon atoms in these compounds form a diverse set of different en-

Compound	Formal C-charge	isoelectronic to	Expected anion structure	ZK rule fulfilled?
Sr_2C	-4	Ne	mono-atomic	Yes
Sr_3C_2	-3	F	dimer	Yes
SrC	-2	O	dimer	Yes
Sr_2C_3	-4/3	N/A	N/A	N/A
SrC_2	-1	N	trigonal non-planar	No
SrC_3	-2/3	N/A	N/A	N/A
Sr_2C_5	-2/5	N/A	N/A	N/A

TABLE I. Applicability of Zintl-Klemm (ZK) rules to the newly identified stoichiometries of strontium carbide. In cases where the formal charge was found to be fractional, the Zintl-Klemm rules cannot be applied ("N/A") in a straightforward manner.

vironments: isolated C atoms in Sr_2C (methanide), dimers in Sr_3C_2 (ethanide) and SrC (ethylenide), linear trimers in Sr_2C_3 (allylenide), chains in SrC , stripes with five-membered (C-pentagons) rings in SrC_2 . There are also infinite ribbons consisting of five-membered (C-pentagons) rings in SrC_3 , ribbons consisting of C-pentagons in SrC_2 , and ribbons made of C-pentagons and C-hexagons in Sr_2C_5 . Bonding patterns in some of the obtained compounds can be described using the Zintl-Klemm rule.

We note that while powerful computational methods, such as evolutionary crystal structure prediction used in this work, are capable of reliably predicting these exotic Sr-C compounds under pressure, experimental validation of the obtained results should be done.

V. ACKNOWLEDGEMENTS

N.R. and A.S. acknowledge funding from the Russian Science Foundation (Project No. 23-13-00332). A.R.O. and P.G. acknowledge funding from the Russian Science Foundation (Project No. 19-72-30043). E.M. thanks the NOMAD Laboratory at the FHI of the Max Planck Society for support of the project.

-
- [1] P. F. McMillan, *Nature materials* **1**, 19 (2002).
- [2] W. Grochala, R. Hoffmann, J. Feng, and N. W. Ashcroft, *Angewandte Chemie International Edition* **46**, 3620 (2007).
- [3] W. Zhang, A. R. Oganov, A. F. Goncharov, Q. Zhu, S. E. Boulfelfel, A. O. Lyakhov, E. Stavrou, M. Somayazulu, V. B. Prakapenka, and Z. Konôpková, *Science* **342**, 1502 (2013).
- [4] X. Dong, A. R. Oganov, A. F. Goncharov, E. Stavrou, S. Lobanov, G. Saleh, G.-R. Qian, Q. Zhu, C. Gatti, V. L. Deringer, *et al.*, *Nature Chemistry* **9**, 440 (2017).
- [5] A. F. Young, C. Sanloup, E. Gregoryanz, S. Scandolo, R. J. Hemley, and H.-k. Mao, *Phys. Rev. Lett.* **96**, 155501 (2006).
- [6] D. V. Semenov, I. A. Kruglov, I. A. Savkin, A. G. Kvashnin, and A. R. Oganov, *Current Opinion in Solid State and Materials Science* **24**, 100808 (2020).
- [7] L. Dubrovinsky, S. Khandarkhaeva, T. Fedotenko, D. Laniel, M. Bykov, C. Giacobbe, E. Lawrence Bright, P. Sedmak, S. Chariton, V. Prakapenka, A. V. Ponomareva, E. A. Smirnova, M. P. Belov, F. Tasnádi, N. Shumlaba, F. Trybel, I. A. Abrikosov, and N. Dubrovinskaia, *Nature* **605**, 274 (2022).
- [8] A. R. Oganov, C. J. Pickard, Q. Zhu, and R. J. Needs, *Nature Reviews Materials* **4**, 331 (2019).
- [9] M. Miao, Y. Sun, E. Zurek, and H. Lin, *Nature Reviews Chemistry* **4**, 508 (2020).
- [10] Y. Ma, M. Erements, A. R. Oganov, Y. Xie, I. Trojan, S. Medvedev, A. O. Lyakhov, M. Valle, and V. Prakapenka, *Nature* **458**, 182 (2009).
- [11] L. Boeri, R. Hennig, P. Hirschfeld, G. Profeta, A. Sanna, E. Zurek, W. E. Pickett, M. Amsler, R. Dias, M. I. Erements, *et al.*, *Journal of Physics: Condensed Matter* **34**, 183002 (2022).
- [12] Q. Zhu, Q. Zeng, and A. R. Oganov, *Physical Review B—Condensed Matter and Materials Physics* **85**, 201407 (2012).
- [13] M. Rice, A. Bishop, and D. Campbell, *Physical review letters* **51**, 2136 (1983).
- [14] R. Hoffmann, C. Janiak, and C. Kollmar, *Macromolecules* **24**, 3725 (1991).
- [15] Z. Wang, X.-F. Zhou, X. Zhang, Q. Zhu, H. Dong, M. Zhao, and A. R. Oganov, *Nano letters* **15**, 6182 (2015).
- [16] Q. Li, Y. Ma, A. R. Oganov, H. Wang, H. Wang, Y. Xu, . f. T. Cui, H.-K. Mao, and G. Zou, *Physical review letters* **102**, 175506 (2009).
- [17] S. E. Boulfelfel, A. R. Oganov, and S. Leoni, *Scientific Reports* **2**, 471 (2012).
- [18] Y. Wang, J. E. Panzik, B. Kiefer, and K. K. Lee, *Scientific reports* **2**, 520 (2012).
- [19] R. Hoffmann and H.-J. Meyer, *Zeitschrift für anorganische und allgemeine Chemie* **607**, 57 (1992).
- [20] C. Su, J. Zhang, G. Liu, X. Wang, H. Wang, and Y. Ma, *Physical Chemistry Chemical Physics* **18**, 14286 (2016).
- [21] M. Krupka, A. Giorgi, N. Krikorian, and E. Szklarz, *Journal of the Less Common Metals* **17**, 91 (1969).
- [22] V. Parasuk and J. Almlöf, *The Journal of chemical physics* **91**, 1137 (1989).
- [23] L. Toth, *Transition metal carbides and nitrides* (Elsevier, 2014).
- [24] F. Spedding, K. Gschneidner Jr, and A. Daane, *Journal of the American Chemical Society* **80**, 4499 (1958).
- [25] T. Sakai, G.-y. Adachi, T. Yoshida, and J. Shiokawa, *The Journal of Chemical Physics* **75**, 3027 (1981).
- [26] R. Rundle, N. Baenziger, A. Wilson, and R. McDonald, *Journal of the American Chemical Society* **70**, 99 (1948).
- [27] F. I. Akbar, A. Aslandukova, Y. Yin, A. Aslandukov, D. Laniel, E. Bykova, M. Bykov, E. L. Bright, J. Wright, D. Comboni, M. Hanfland, N. Dubrovinskaia, and L. Dubrovinsky, *Carbon* **228**, 119374 (2024).
- [28] X. Feng, S. Lu, C. J. Pickard, H. Liu, S. A. Redfern, and Y. Ma, *Communications Chemistry* **1**, 85 (2018).
- [29] R. West, P. A. Carney, and I. Mineo, *Journal of the American Chemical Society* **87**, 3788 (1965).
- [30] H. Mattausch, T. Gulden, R. K. Kremer, J. Horakh, and A. Simon, *Zeitschrift für Naturforschung B* **49**, 1439 (1994).
- [31] H. Fjellvaag and P. Karen, *Inorganic Chemistry* **31**, 3260 (1992).
- [32] R. Poettgen and W. Jeitschko, *Inorganic Chemistry* **30**, 427 (1991).
- [33] T. A. Strobel, O. O. Kurakevych, D. Y. Kim, Y. Le Godec, W. Crichton, J. Guignard, N. Guignot, G. D. Cody, and A. R. Oganov, *Inorganic Chemistry* **53**, 7020 (2014).
- [34] Y.-L. Li, S.-N. Wang, A. R. Oganov, H. Gou, J. S. Smith, and T. A. Strobel, *Nature Communications* **6**, 6974 (2015).
- [35] S. Khandarkhaeva, T. Fedotenko, A. Aslandukova, F. I. Akbar, M. Bykov, D. Laniel, A. Aslandukov, U. Ruschewitz, C. Tobeck, B. Winkler, S. Chariton, V. Prakapenka, K. Glazyrin, C. Giacobbe, E. L. Bright, M. Belov, N. Dubrovinskaia, and L. Dubrovinsky, *Nature Communications* **15**, 2855 (2024).
- [36] S. Roszak and K. Balasubramanian, *The Journal of Physical Chemistry* **100**, 8254 (1996).
- [37] A. Aslandukova, A. Aslandukov, L. Yuan, D. Laniel, S. Khandarkhaeva, T. Fedotenko, G. Steinle-Neumann, K. Glazyrin, N. Dubrovinskaia, and L. Dubrovinsky, *Phys. Rev. Lett.* **127**, 135501 (2021).
- [38] X. Gao, Y. Jiang, R. Zhou, and J. Feng, *Journal of Alloys and Compounds* **587**, 819 (2014).
- [39] D. Young Kim, P. Srepusharawoot, C. J. Pickard, R. J. Needs, T. Bovornratanaraks, R. Ahuja, and U. Pinsook, *Applied Physics Letters* **101** (2012).
- [40] P. Tsuppayakorn-Aek, W. Chaimayo, U. Pinsook, and T. Bovornratanaraks, *AIP Advances* **5** (2015).
- [41] A. R. Oganov, A. O. Lyakhov, and M. Valle, *Accounts of Chemical Research* **44**, 227 (2011), pMID: 21361336, <https://doi.org/10.1021/ar1001318>.
- [42] N. Rybin, D. Y. Novoselov, D. M. Korotin, V. I. Anisimov, and A. R. Oganov, *Phys. Chem. Chem. Phys.* **23**, 15989 (2021).
- [43] N. Rybin, I. Chepkasov, D. Y. Novoselov, V. I. Anisimov, and A. R. Oganov, *The Journal of Physical Chemistry C* **126**, 15057 (2022), <https://doi.org/10.1021/acs.jpcc.2c04785>.
- [44] C. W. Glass, A. R. Oganov, and N. Hansen, *Computer physics communications* **175**, 713 (2006).
- [45] A. R. Oganov and C. W. Glass, *The Journal of Chemical Physics* **124**, 244704 (2006).

- [46] A. O. Lyakhov, A. R. Oganov, H. T. Stokes, and Q. Zhu, *Computer Physics Communications* **184**, 1172 (2013).
- [47] A. Jain, S. P. Ong, W. Chen, B. Medasani, X. Qu, M. Kocher, M. Brafman, G. Petretto, G.-M. Rignanese, G. Hautier, D. Gunter, and K. A. Persson, *Concurrency and Computation: Practice and Experience* **27**, 5037 (2015), <https://onlinelibrary.wiley.com/doi/pdf/10.1002/cpe.3505>.
- [48] D. M. Deaven and K. M. Ho, *Phys. Rev. Lett.* **75**, 288 (1995).
- [49] J. P. Perdew, K. Burke, and M. Ernzerhof, *Physical Review Letters* **77**, 3865 (1996).
- [50] P. Giannozzi, S. Baroni, N. Bonini, M. Calandra, R. Car, C. Cavazzoni, D. Ceresoli, G. L. Chiarotti, M. Cococcioni, I. Dabo, *et al.*, *Journal of physics: Condensed matter* **21**, 395502 (2009).
- [51] P. Giannozzi *et al.*, *Journal of Physics: Condensed Matter* **29**, 465901 (2017).
- [52] G. Kresse and J. Furthmüller, *Physical Review B* **54**, 11169 (1996).
- [53] P. E. Blöchl, *Physical Review B* **50**, 17953 (1994).
- [54] S. Fredericks, K. Parrish, D. Sayre, and Q. Zhu, *Computer Physics Communications* **261**, 107810 (2021).
- [55] P. V. Bushlanov, V. A. Blatov, and A. R. Oganov, *Computer Physics Communications* **236**, 1 (2019).
- [56] K. Parlinski, Z. Q. Li, and Y. Kawazoe, *Phys. Rev. Lett.* **78**, 4063 (1997).
- [57] A. Togo and I. Tanaka, *Scripta Materialia* **108**, 1 (2015).
- [58] K. Momma and F. Izumi, *Journal of applied crystallography* **44**, 1272 (2011).
- [59] G. Henkelman, A. Arnaldsson, and H. Jónsson, *Computational Materials Science* **36**, 354 (2006).
- [60] M. Yu and D. R. Trinkle, *The Journal of chemical physics* **134** (2011).
- [61] E. Sanville, S. D. Kenny, R. Smith, and G. Henkelman, *Journal of computational chemistry* **28**, 899 (2007).
- [62] W. Tang, E. Sanville, and G. Henkelman, *Journal of Physics: Condensed Matter* **21**, 084204 (2009).
- [63] O. O. Kurakevych, T. A. Strobel, D. Y. Kim, and G. D. Cody, *Angewandte Chemie International Edition* **52**, 8930 (2013).
- [64] W. Zachariasen, *Acta Crystallographica* **1**, 265 (1948).
- [65] A. Riabov, V. Yartys, B. Hauback, P. Guegan, G. Wiesinger, and I. Harris, *Journal of alloys and compounds* **293**, 93 (1999).
- [66] P. Chai and J. D. Corbett, *Acta Crystallographica Section C: Crystal Structure Communications* **67**, i53 (2011).
- [67] A. Almenningen, O. Bastiansen, and M. Traetteberg, *Acta Chemica Scandinavica* **13**, 1699 (1959).
- [68] F. I. Akbar, A. Aslandukova, Y. Yin, A. Aslandukov, D. Laniel, E. Bykova, M. Bykov, E. L. Bright, J. Wright, D. Comboni, *et al.*, *Carbon*, 119374 (2024).

Novel Strontium Carbides Under Compression

Supplementary Information

Nikita Rybin,^{*,†} Evgeny Moerman,[¶] Pranab Gain,[†] Artem Oganov,[†] and
Alexander Shapeev^{*,†}

[†]*Skolkovo Institute of Science and Technology, Bolshoi bulvar 30, build.1, 121205, Moscow*

[‡]*Digital Materials LLC, Medovaya 3, 143085, Moscow Region*

[¶]*Molecular Simulations from First Principles e.V., D-14195 Berlin, Germany*

E-mail: n.rybin@skoltech.ru; a.shapeev@skoltech.ru

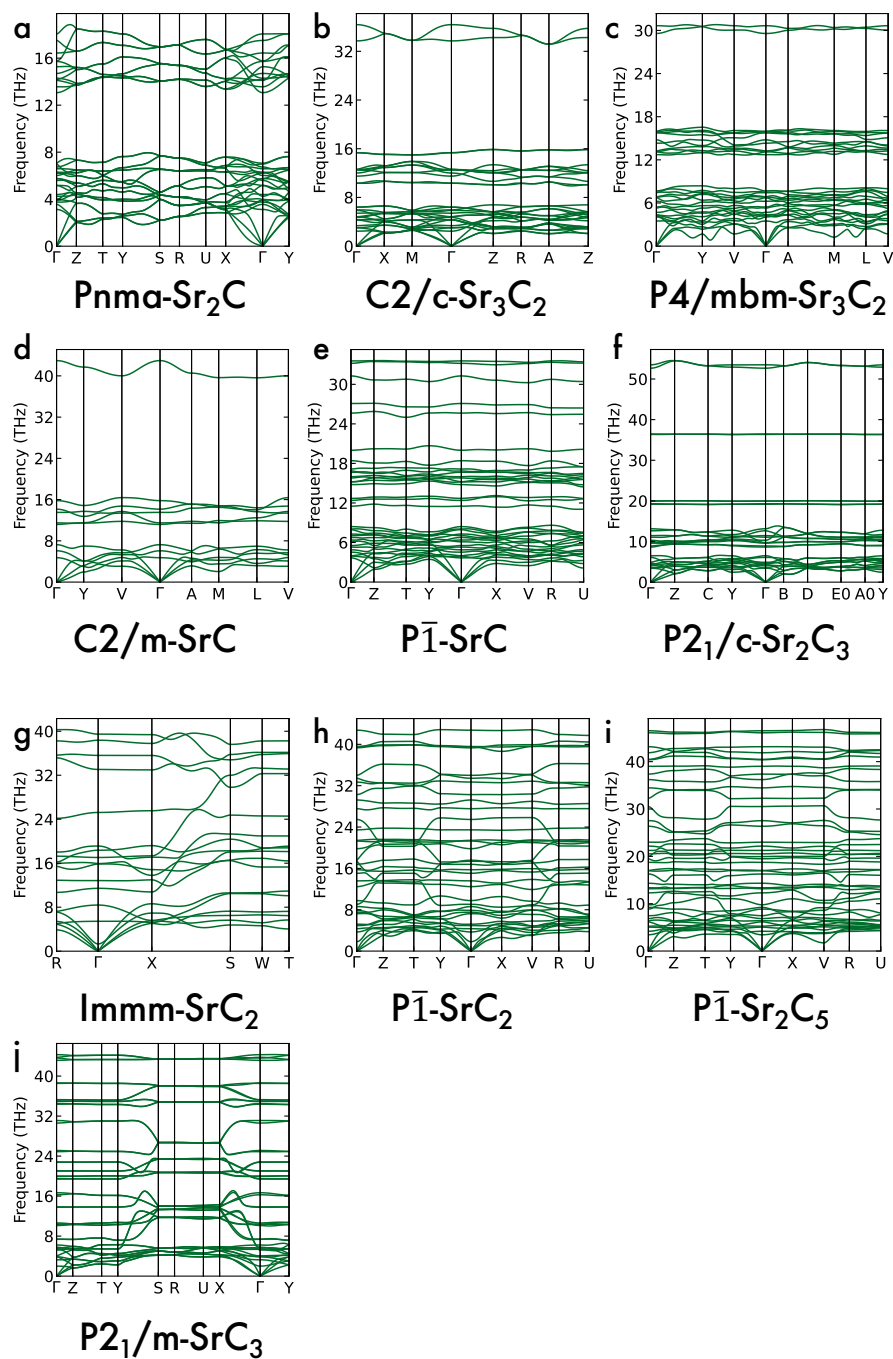


Figure S1: Phonon dispersion curves for discovered Sr-C compounds.

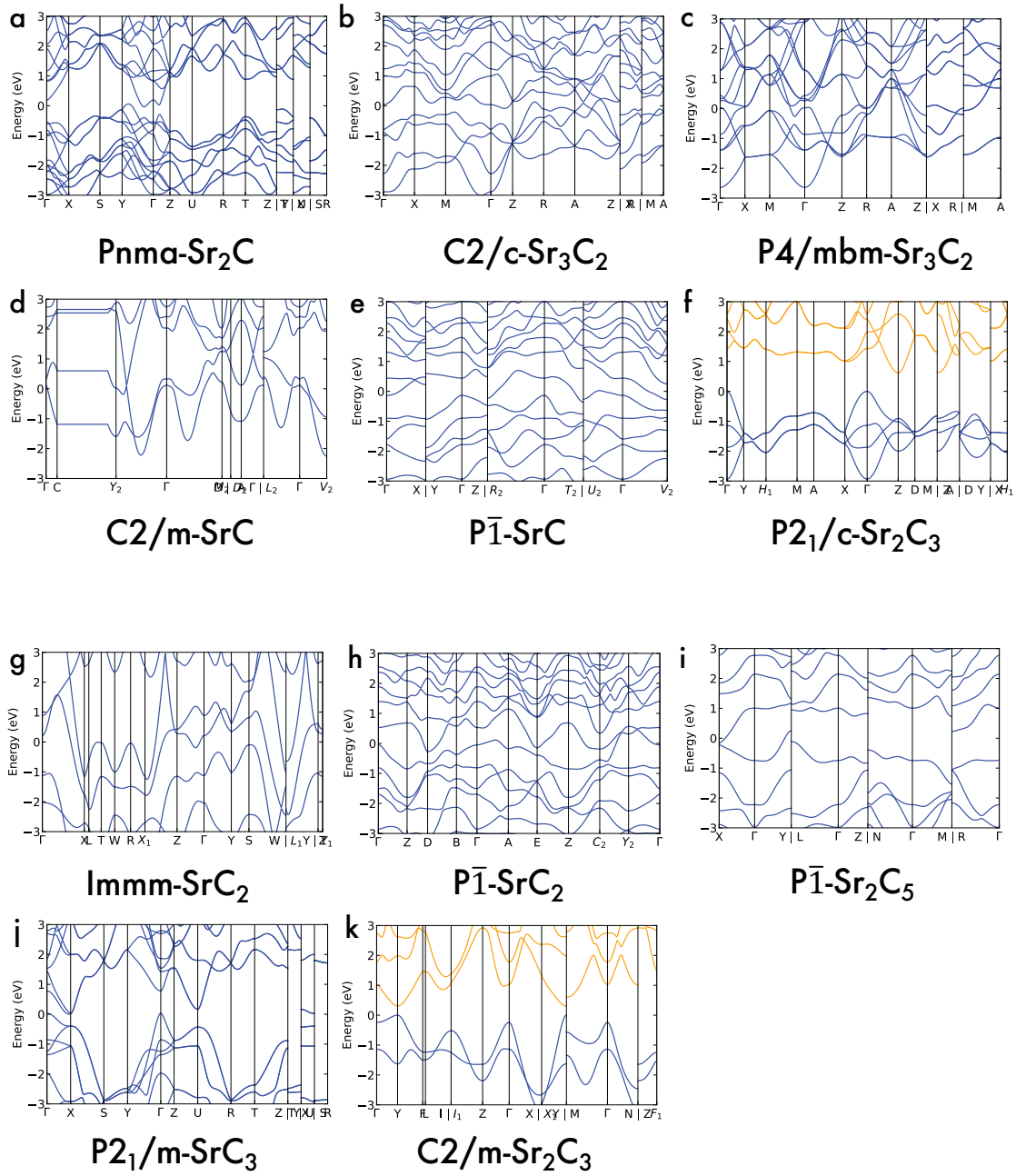


Figure S2: Band structures for discovered Sr-C compounds.

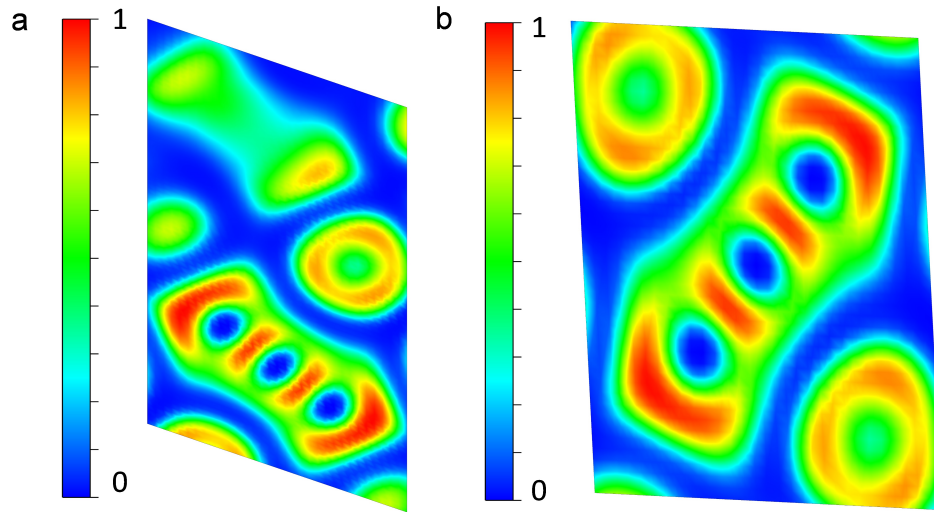


Figure S3: 2D electron localization function of (a) $C2/m$ - Sr_2C_3 structure at 20 GPa and (b) $P2_1/c$ - Sr_2C_3 structure at 30 GPa, showing the covalent bonding between the carbon atoms and ionic interaction between Sr and C atoms.

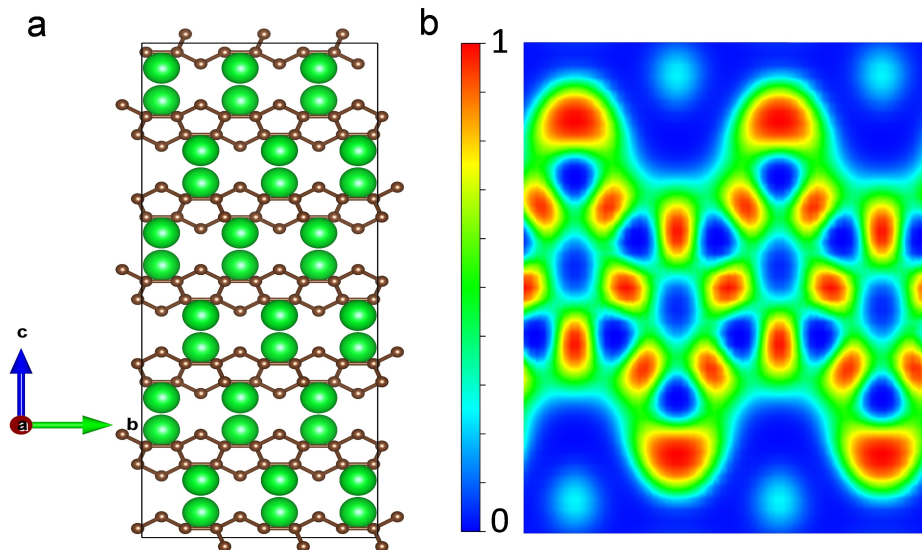


Figure S4: (a) The crystal structure of SrC_3 viewed along a-direction showing the infinite pentagonal ribbons (b) The 2D electron localization function containing the carbon ribbons

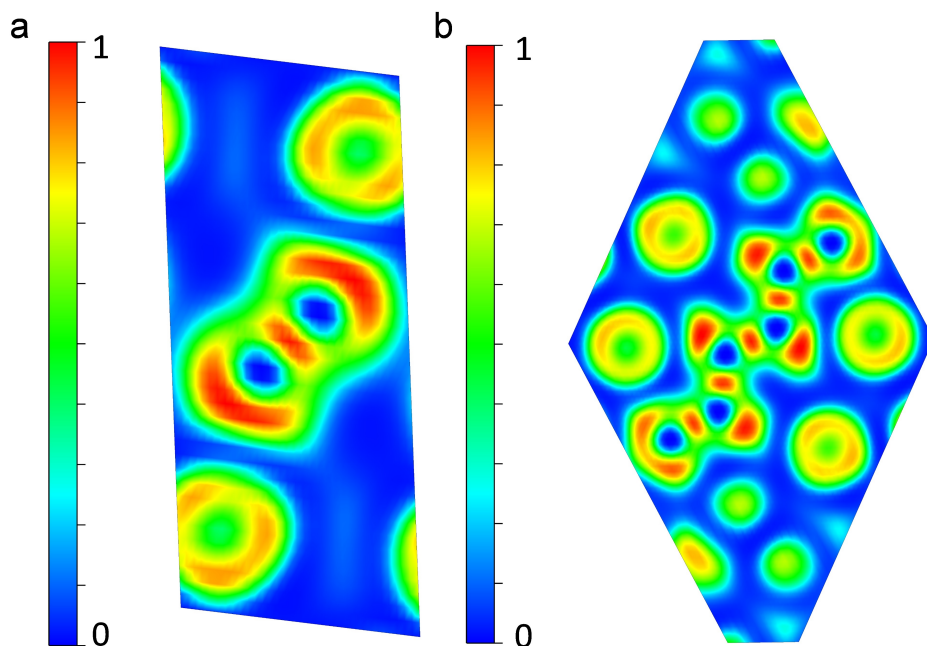


Figure S5: The 2D Electron Localization Function (ELF) shows (a) electron density localization around the C-dimer in $C2/m$ -SrC at 30 GPa, and (b) around the 6-atom carbon chain in $P\bar{1}$ -SrC at 50 GPa. Both ELF's indicate ionic Sr-C interactions and covalent bonding between carbon atoms.

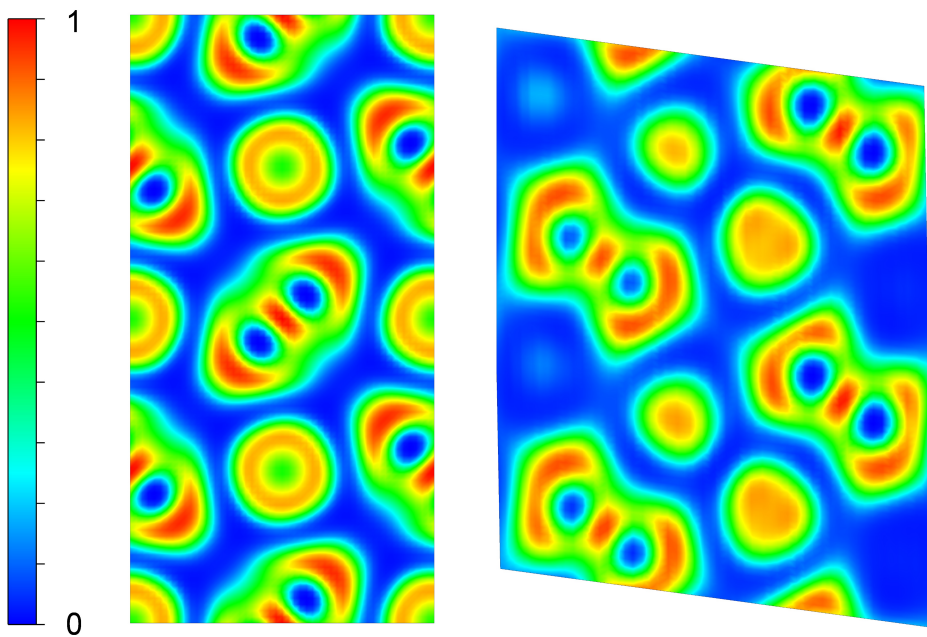


Figure S6: The 2D Electron Localization Function (ELF) containing the C_2 dimers in $P4/mbm$ - Sr_3C_2 (left) at 30GPa and in $C2/c$ - Sr_3C_2 (right) at 50 GPa.

Supplementary Table 1. Crystal structures and Bader analyses of stable Sr-C compounds at various pressures.

Pressure (GPa)	Space group	Lattice parameters					Atomic fractional coordinates			Bader ($ e $, Å ³)	
		a	b	c	α	β	γ	Å	°	Charge	Volume

Sr₂C

50	<i>Pnma</i> (62)	5.7173 90	4.0570 90	7.5693 90	Sr1 1a	0.0169	0.2500	0.8191	0.998	14.622
					Sr2 1a	0.4831	0.7500	0.3192	0.998	14.623
					Sr3 1a	0.6614	0.2500	0.0857	0.997	14.211
					Sr4 1a	0.3386	0.7500	0.9143	0.997	14.211
					Sr5 1a	0.9831	0.7500	0.1808	0.998	14.621
					Sr6 1a	0.1614	0.2500	0.4143	0.997	14.210
					Sr7 1a	0.5169	0.2500	0.6808	0.998	14.623
					Sr8 1a	0.8386	0.7500	0.5857	0.997	14.211
					C1 1a	0.2342	0.2500	0.0978	-1.993	15.060
					C2 1a	0.7658	0.7500	0.9022	-1.993	15.059
					C3 1a	0.2658	0.7500	0.5978	-1.993	15.059
					C4 1a	0.7348	0.2500	0.4022	-1.993	15.059

Sr₃C₂

30	<i>P4/mbm</i> (127)	6.1466 90	6.1466 90	4.0944 90	Sr1 1a	0.1757	0.6757	0.0000	0.873	16.596					
					Sr2 1a	0.8243	0.3243	0.0000	0.873	16.586					
					Sr3 1a	0.5000	0.5000	0.5000	0.701	17.706					
					Sr4 1a	0.6757	0.8243	0.0000	0.873	16.586					
					Sr5 1a	0.3243	0.1757	0.0000	0.873	16.593					
					Sr6 1a	0.0000	0.0000	0.5000	0.701	17.706					
					C1 1a	0.0799	0.4201	0.5000	-1.163	13.092					
					C2 1a	0.4201	0.9201	0.5000	-1.163	13.092					
					C3 1a	0.5799	0.0799	0.5000	-1.293	13.368					
					C4 1a	0.9201	0.5799	0.5000	-1.293	13.368					
					50	<i>C2/c</i> (15)	4.5489 100.69	4.5489 100.69	6.6225 91.13	Sr1 1a	0.7395	0.6729	0.9749	0.751	15.046
										Sr2 1a	0.8154	0.1846	0.2500	0.766	15.200
										Sr3 1a	0.2605	0.3271	0.0251	0.750	15.045
Sr4 1a	0.1846	0.8154	0.7500	0.766						15.200					
Sr5 1a	0.6729	0.7395	0.4749	0.873						16.593					
Sr6 1a	0.3271	0.2605	0.5251	0.750						15.045					
C1 1a	0.1274	0.7279	0.3187	-1.137						10.387					
C2 1a	0.2721	0.8726	0.1813	-1.129						10.375					
C3 1a	0.7277	0.1274	0.8187	-1.137						10.387					
C4 1a	0.8726	0.2721	0.6813	-1.129						10.375					

SrC

30	<i>C2m</i> (12)	4.749	4.749	3.822	Sr1 1a	0.8556	0.8556	0.8116	1.089	15.527
		98.56	98.56	41.11	Sr2 1a	0.1444	0.1444	0.1884	1.087	15.534
					C1 1a	0.4387	0.4387	0.3726	-1.131	12.517
					C2 1a	0.5613	0.5613	0.6274	-1.044	13.803
50	<i>P-1</i> (2)	4.637	4.900	6.948	Sr1 1a	0.3343	0.1846	0.0239	1.059	13.397
		99.18	105.87	103.84	Sr2 1a	0.3052	0.3935	0.6137	0.996	14.201
					Sr3 1a	0.7789	0.1225	0.6820	0.998	13.753
					Sr4 1a	0.6948	0.6065	0.3863	0.996	14.201
					Sr5 1a	0.2212	0.8775	0.3180	0.998	13.753
					Sr6 1a	0.6658	0.8154	0.9760	1.059	13.397
					C1 1a	0.2053	0.8646	0.6759	-1.306	11.346
					C2 1a	0.0039	0.6894	0.7666	-0.863	9.374
					C3 1a	0.1140	0.5888	0.9593	-0.874	9.475
					C4 1a	0.9961	0.3106	0.2334	-0.863	9.374
					C5 1a	0.8860	0.4112	0.0407	-0.893	9.501
					C6 1a	0.7947	0.1354	0.3241	-1.306	11.346

Sr₂C₃

20	<i>C2m</i> (12)	5.2644	5.2644	3.9054	Sr1 1a	0.8664	0.8664	0.7959	1.314	15.842
		94.90	94.90	40.08	Sr2 1a	0.1336	0.1336	0.2041	1.314	15.848
					C1 1a	0.5000	0.5000	0.5000	-1.225	10.106
					C2 1a	0.6118	0.6118	0.7096	-0.700	13.803
					C3 1a	0.3882	0.3882	0.2905	-0.701	13.803
30	<i>P2₁/c</i>	3.8018	5.2946	7.0634	Sr1 1a	0.8039	0.6392	0.8192	1.310	16.287
		90	90	90	Sr2 1a	0.1961	0.3608	0.1809	1.310	16.287
					Sr3 1a	0.1969	0.1392	0.6808	1.310	16.287
					Sr4 1a	0.8039	0.8608	0.3192	1.310	16.287
					C1 1a	0.3150	0.6951	0.5564	-0.761	14.142
					C2 1a	0.6850	0.3050	0.4406	-0.761	14.142
					C3 1a	0.5000	0.5000	0.5000	-1.098	10.232
					C4 1a	0.6850	0.1951	0.9406	-0.761	14.142
					C5 1a	0.5000	0.0000	0.0000	-1.098	10.232
					C6 1a	0.8039	0.6392	0.8192	-0.761	14.142

SrC₂

50	<i>P-1</i> (2)	4.7266	4.9967	5.8029	Sr1 1a	0.6899	0.2924	0.2344	1.155	13.818
		112.16	102.75	98.98	Sr2 1a	0.3101	0.7076	0.7656	1.155	13.818
					Sr3 1a	0.2926	0.6583	0.2578	1.177	13.478
					Sr4 1a	0.7074	0.3417	0.7422	1.177	13.478
					C1 1a	0.8685	0.8791	0.4372	-0.440	6.904
					C2 1a	0.9827	0.2200	0.8823	-0.388	6.993
					C3 1a	0.2279	0.2036	0.3732	-0.771	9.313
					C4 1a	0.7792	0.7816	0.1570	-0.768	9.220
					C5 1a	0.1315	0.1209	0.5628	-0.407	6.863
					C6 1a	0.0173	0.9781	0.1177	-0.349	6.940
					C7 1a	0.2208	0.2184	0.8430	-0.770	9.234

			C8 1a	0.7721	0.7964	0.6268	-0.771	9.311
90	<i>Immm</i> (71)	4.7364 4.7364 4.7364 148.94 103.07 85.25	Sr1 1a	0.2041	0.7041	0.5000	1.134	11.859
			Sr2 1a	0.7960	0.2960	0.5000	1.134	11.859
			C1 1a	0.2599	0.0000	0.2599	-0.743	7.903
			C2 1a	0.7402	0.0000	0.7402	-0.746	7.918
			C3 1a	0.6220	0.5000	0.1220	-0.368	6.243
			C4 1a	0.3780	0.5000	0.8780	-0.413	6.316

Sr₂C₅

60	<i>P 1</i> (1)	4.7994 4.8591 5.9612 71.11 82.46 79.13	Sr1 1a	0.3654	0.2722	0.3174	1.202	13.180
			Sr2 1a	0.2643	0.3296	0.8241	1.248	13.375
			Sr3 1a	0.7357	0.6704	0.1759	1.248	13.375
			Sr4 1a	0.6346	0.7278	0.6825	1.202	13.179
			C1 1a	0.7332	0.2699	0.5777	-0.577	8.763
			C2 1a	0.9269	0.1009	0.1971	-0.423	6.871
			C3 1a	0.8974	0.1134	0.4333	-0.423	6.553
			C4 1a	0.1648	0.8692	0.1937	-0.336	6.673
			C5 1a	0.8352	0.1308	0.8064	-0.336	6.673
			C6 1a	0.2496	0.7550	0.9974	-0.705	9.002
			C7 1a	0.1026	0.8866	0.5666	-0.393	6.519
			C8 1a	0.7504	0.2450	0.0026	-0.705	9.002
			C9 1a	0.0731	0.8991	0.8026	-0.423	6.872
			C10 1a	0.2668	0.7301	0.4223	-0.577	8.764

SrC₃

20	<i>Pnma</i> (62)	5.1131 3.6431 9.1203 90 90 90	Sr1 1a	0.8999	0.7500	0.3483	1.343	15.506
			Sr2 1a	0.1000	0.2500	0.6517	1.343	15.506
			Sr3 1a	0.6000	0.2500	0.8483	1.343	15.506
			Sr4 1a	0.3999	0.7500	0.1517	1.343	15.506
			C1 1a	0.5972	0.0532	0.5550	-0.437	7.905
			C2 1a	0.4028	0.5532	0.4450	-0.279	7.520
			C3 1a	0.9721	0.4468	0.9450	-0.244	7.475
			C4 1a	0.9028	0.9468	0.0550	-0.437	7.905
			C5 1a	0.2301	0.7500	0.8740	-0.662	11.587
			C6 1a	0.9028	0.5532	0.0550	-0.279	7.520
			C7 1a	0.7699	0.2500	0.1260	-0.662	11.587
			C8 1a	0.0972	0.0532	0.9450	-0.402	7.859
			C9 1a	0.2699	0.2500	0.3740	-0.662	11.587
			C10 1a	0.5972	0.4468	0.5550	-0.244	7.475
			C11 1a	0.7302	0.7500	0.6260	-0.662	11.587
			C12 1a	0.4028	0.9468	0.4450	-0.402	7.859